Variability of the Horizontal Velocity Structure in the Upper 1600 m of the Water Column on the Equator at 10°W

LUCIA BUNGE,* CHRISTINE PROVOST, AND JONATHAN M. LILLY

LODYC, UMR 7617, CNRS/IRD/UPMC/MNHN, Université Pierre et Marie Curie, Paris, France

MARC D'ORGEVILLE

LPO, UMR 6523, CNRS/IFREMER/UBO, Plouzané, France

ANNIE KARTAVTSEFF

LODYC, UMR 7617, CNRS/IRD/UPMC/MNHN, Université Pierre et Marie Curie, Paris, France

JEAN-LUC MELICE

Institut de Recherche pour le Developpement, Oceanography Department, University of Cape Town, Rondebosch, South Africa

(Manuscript received 29 March 2004, in final form 7 October 2005)

ABSTRACT

This paper presents initial results from new velocity observations in the eastern part of the equatorial Atlantic Ocean from a moored current-meter array. During the "EQUALANT" program (1999–2000), a mooring array was deployed around the equator near 10°W that recorded one year of measurements at various depths. Horizontal velocities were obtained in the upper 60 m from an upward-looking acoustic Doppler current profiler (ADCP) and at 13 deeper levels from current meters between 745 and 1525 m. To analyze the quasiperiodic variability observed in these records, a wavelet-based technique was used. Quasiperiodic oscillations having periods between 5 and 100 days were separated into four bands: 5–10, 10–20, 20–40, and 40–100 days. The variability shows (i) a strong seasonality (the first half of the series is dominated by larger periods than the second one) and (ii) a strong dependence with depth (some oscillations are present in the entire water column while others are only present at certain depths). For the oscillations that are present in the entire water column the origin of the forcing can be traced to the surface, while for the others the question of their origin remains open. Phase shifts at different depths generate vertical shears in the horizontal velocity component with relatively short vertical scales. This is especially visible in long-duration events (>100 days) of the zonal velocity component. Comparison with a simultaneous lowered acoustic Doppler current profiler (LADCP) section suggests that some of these flows may be identified with equatorial deep jets. A striking feature is a strong vertical shear lasting about 7 months between 745 and 1000 m. These deep current-meter observations would then imply a few months of duration for the jets in this region.

1. Introduction

Signals propagate much faster in the equatorial region than in the rest of the ocean. Tropical oceans therefore play an important climatic role at relatively short time scales. Velocity measurements at the equator have shown very high horizontal velocities, a wide range of variability, and different spectral contents for the two horizontal velocity components, with zonal motions being dominated by longer periods than meridional motions (e.g., Weisberg and Horigan 1981).

In the equatorial Atlantic Ocean, velocity measurements are rather sparse in time and space. Near the surface, they come from ship drifts (e.g., Richardson and Walsh 1986) and drifting buoys (e.g., Lumpkin and Garzoli 2005), as well as from numerous inverted echosounders and current meters deployed as part of the

* Current affiliation: Department of Oceanography, The Florida State University, Tallahassee, Florida.

Corresponding author address: Lucia Bunge, Department of Oceanography, The Florida State University, Tallahassee, FL 32306-4320.
E-mail: bunge@ocean.fsu.edu

© 2006 American Meteorological Society

Francais Ocean et Climat dans l'Atlantique Equatorial-Seasonal Equatorial Atlantic Experiment (FOCAL-SEQUAL) (1982–84) (e.g., Garzoli 1987; Houghton and Colin 1987; Weisberg and Weingartner 1988). Intermediate depths were sampled in the Gulf of Guinea by current-meter moorings during a U.S.–French cooperative program that lasted from June 1976 to May 1978 (Weisberg and Horigan 1981). Deep velocity time series were also obtained from moorings at 36°W (Send et al. 2002) and at the Romanche fracture zone (Mercier and Speer 1998; Thierry et al. 2006) between 1992 and 1994. Additionally, some floats have documented the velocity field around 1000 m (e.g., Richardson and Schmitz 1993; Molinari et al. 1999; Boebel et al. 1999; Schmid et al. 2003), and lowered acoustic Doppler current profilers (LADCPs) have returned velocity sections throughout the entire water column during several hydrographic cruises (e.g., Gouriou et al. 2001; Bourlès et al. 2003).

Most studies of oceanic signals at the equator have tried to relate them to linear equatorial waves. One of the dominant periods in the meridional velocity component at the surface is about 30 days, associated with tropical instability waves (Weisberg and Weingartner 1988). These waves are usually present from June to October (e.g., Grodsky et al. 2005), and their expression below the thermocline resembles that of linear Rossby–gravity waves (Weisberg et al. 1979). In the eastern part of the basin, energetic oscillations having a 14-day period are also observed in near-surface oceanic records by Garzoli (1987) and Houghton and Colin (1987). Garzoli (1987) surmised that these oscillations are forced by wind fluctuations at the same period in the zonal wind component. The maximum amplitude of the 14-day signal was found to occur in the mixed layer at 3°N, which does not agree with equatorial wave theory that implies symmetry about the equator. Houghton and Colin (1987), on the other hand, attribute the forcing to the meridional wind velocity component and found that the thermocline displacements are nearly antisymmetric about the equator and that the structure of the oscillation resembles that of a second baroclinic mode Rossby–gravity wave.

At depth, the zonal velocity component is dominated by lower frequencies (~66 days, semiannual, annual, and interannual oscillations) that, in some cases, have Rossby and/or Kelvin wave characteristics (e.g., Thierry 2000; Schmid et al. 2003).

Among the most remarkable features of the deep equatorial scenario are the equatorial deep jets (EDJs) that are present in the zonal velocity component between the thermocline and 2500 m. First discovered in the Indian Ocean by Luyten and Swallow (1976), they have been observed in the Pacific (Eriksen 1985; Firing 1987) as well as in the Atlantic (Ponte et al. 1990; Gouriou et al. 1999; Send et al. 2002; Bourlès et al. 2003). In the Atlantic Ocean, EDJs have vertical scales of around 400–600 m and a typical meridional extent of 1° (e.g., Gouriou et al. 1999).

There is no general consensus on whether EDJs are the result of equatorial Kelvin waves or first meridional-mode equatorial Rossby waves, if any wave at all. Certain characteristics like the high zonal velocities are indicators of Kelvin wave behavior but others, like the potential vorticity structure (Muench et al. 1994) or the off-equatorial maxima of vertical strain (Johnson and Zhang 2003), suggest similarities with Rossby waves. In any case, the scales do not seem to match those of linear theory and thus nonlinearities have been suggested (Weisberg and Horigan 1981; Philander 1990; Hua et al. 1997). Another unknown is the temporal scale of these structures. Gouriou et al. (1999) suggest a seasonal reversal of the jets but, as other authors have recently remarked (e.g., Send et al. 2002), vertically propagating energy at large vertical scales could be responsible for such apparent jet reversals. Based on linear wave theory, Johnson and Zhang (2003) propose periods of at least 5 years. Send et al. (2002) estimate similar periods, but also pointed out the possibility of an intermittent behavior.

Here we report the initial results from a mooring array deployed at 10°W and the equator during the "EQUALANT" program (1999–2000). The year-long dataset consist of horizontal velocities in the upper 60 m obtained with an upward-looking ADCP and the same at 13 deeper levels from current meters placed at depths between 745 and 1525 m. Despite the absence of data between 60 and 745 m, the EQUALANT current-meter dataset is unique because of its high vertical resolution between 745 and 1525 m. These depths are characterized by the presence of EDJs and by the interface between two important water masses: Antarctic Intermediate Water (AAIW) and North Atlantic Deep Water (NADW).

The objective of this paper is to provide a first description of these new data and to discuss the major features in comparison with previous observations and theory. Because the data clearly contain quasiperiodic fluctuations that may be modulated in time or may occur only in certain portions of a time series, we use a wavelet-based technique (see the appendix) to isolate and extract individual component signals. It is found that energetic fluctuations occur both at the surface and at depth, often with similar periods. These fluctuations are either distributed uniformly with depth or are con-

centrated at a few distinct depth ranges. We find long-duration events with vertical scales comparable to those of EDJs and temporal scales on the order of 7 months.

The paper is organized as follows: section 2 describes the data and experiment, section 3 the wavelet method, and section 4 the general spectral characteristics of the data and the main oscillations observed; section 5 analyzes the vertical scales of long duration events, and the results are summarized and discussed in section 6.

2. Data

Current-meter data were obtained from 16 vector-averaging current meters (VACMs) and a 150-kHz narrowband acoustic Doppler current profiler (ADCP), deployed on/near the equator at 10°W from November 1999 to November 2000 as part of the EQUALANT program (information available online at http://nansen.ipsl.jussieu.fr/EQUALANT; Kartavtseff 2002). The array was initially designed with four moorings (Fig. 1) of four VACMs each to sample the water column between 1000- and 1600-m depth. Two moorings were placed exactly on the equator (moorings A and Y), one at 0.75°N (mooring N), and one at 0.75°S (mooring S). Mooring A on the equator was equipped with an ADCP to sample the surface and subsurface. It was deployed with a parachute to reduce the tension of the cable. This technique, while it made the mooring descend gently, also let the mooring drift to a somewhat shallower location than was originally planned. As a result, the ADCP was only able to continuously sample the upper 50–60 m (Fig. 2). Mooring Y had VACMs at staggered depths with those of mooring A in order to increase vertical resolution. An intermediate cruise was done in March 2000 to recover and redeploy mooring Y. The recovery of the whole array was done in November 2000.

Table 1 reports the depth and duration of the current-meter time series: Y_A and Y_B represent the two deployments of mooring Y and the numbers 1, 2, 3, 4 after the mooring's designation represent the current meters by order of increasing depth. Furthermore, series from Y_A at 1187 and 1420 m were merged with series Y_B at 1190 and 1415 m to form series Y2 and Y3, respectively, while Y_B at 930 was named Y1. Henceforth, we will use the 30-m-depth ADCP time series as a representation of near-surface data. Because of technical problems with some of the VACMs, only 13 series were analyzed, the length of the longest time series being 380 days (see Table 1 for details). To examine time scales of variability longer than one week, the hourly data were averaged every 25 h to remove tidal frequencies and resampled to daily resolution (Fig. 3).

The VACMs were calibrated both before and after

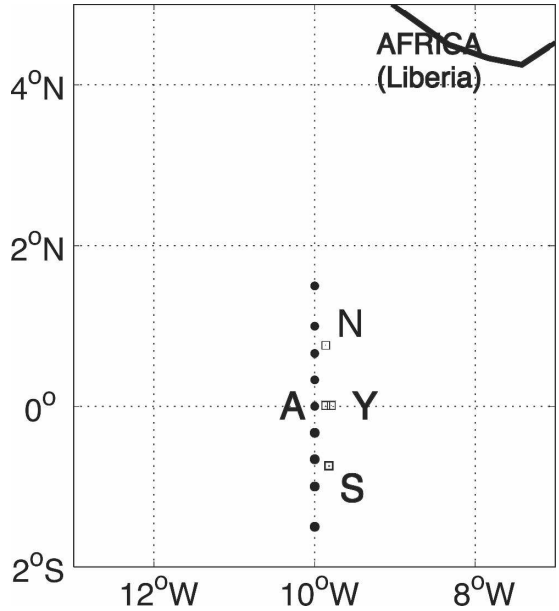

FIG. 1. Study area. Squares indicate the position of the four moorings: two on the equator (A and Y), one at 0.75°N (N), and one at 0.75°S (S). Mooring A has an ADCP to measure the subsurface and it is placed just next to a PIRATA ATLAS buoy. The instruments were in the water from Nov 1999 to Nov 2000. Solid circles indicate the location of some of the EQUALANT LADCP sections used in this paper made during 30 Jul and 1 Aug 2000.

deployment at the Institut français de recherche pour l'exploitation de la mer (Ifremer) in Brest, France. The reported accuracies are within the range of ±1–2 cm s^{-1} for the various instruments, with the minimum measurable current speeds varying between 0.53 and 3.78 cm s^{-1}.

The analysis also makes use of lowered acoustic Doppler current profiler (LADCP) data collected during the EQUALANT cruise in July and August 2000 (Fig. 4), while the current meters were in the water. These data have been previously described in Bourlès et al. (2003).

To investigate possible forcing mechanisms for the variability observed, surface wind data were also analyzed. Wind data came from two sources: satellite scatterometer data from the National Aeronautics and Space Administration Quick Scatterometer (QuikSCAT) (information available online at http://www.ifremer.fr/cersat/fr/data/overview/gridded/mwfqscat.htm) between 20 July 1999 and 20 May 2004, and from the Autonomous Temperature Line Acquisition System (ATLAS) buoy of the Pilot Research Moored Array in the Tropical Atlantic (PIRATA) at 10°W (see information online at http://www.pmel.noaa.gov/pirata/display.html).

The satellite scatterometer data have a daily tempo-

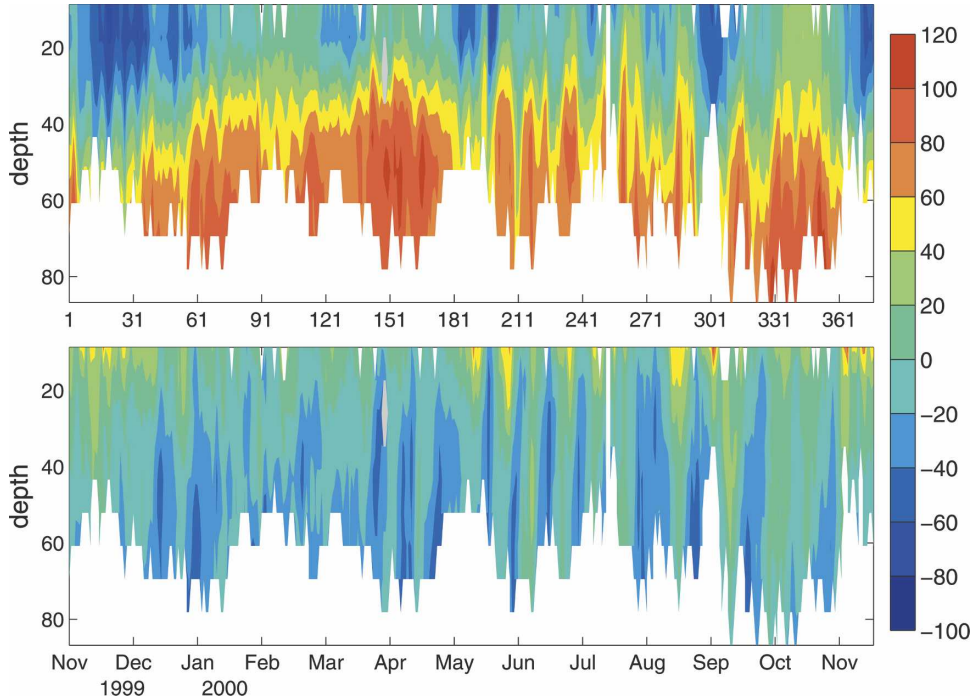

FIG. 2. (top) Zonal and (bottom) meridional velocity components (cm s^{-1}) from the ADCP in mooring A. Time axis is in days (top) and in months (bottom), beginning on 12 Nov 1999 and ending 24 Nov 2000.

ral resolution and a 0.5° spatial resolution. We examined the region between 7.25°S and 9.25°N, 25.75° and 0.25°W. Because of the large size of this dataset, the analysis was performed with a multitaper method (MTM) (Thomson 1982; Percival and Walden 1993). We used the singular spectrum analysis (SSA) MTM toolkit (Ghil et al. 2002) with nine tapers: $9 = 2P - 1$, where P is the time bandwidth product. The smoothing of the spectrum may be estimated by $2P/N$, where N is the time length of the series (almost 5 years). This implies a smoothing in Fourier space over a region of approximately two cycles per year in width. The spatial distribution of the oscillations representing the "peaks" in the spectra (Fig. 5b) shows maps of the spectrum amplitudes corresponding to some of those periods (Figs. 5c and 5d).

TABLE 1. Depth and duration of the current-meter time series. The moorings were deployed between 11 Nov 1999 and 24 Nov 2000. The location is given by the capital letters: N is 0.75°N, S is 0.75°S, A and Y are the very equator; Y_A and Y_B represent the two deployments of mooring Y. The numbers 1, 2, 3, and 4 represent the instruments on each mooring in increasing order of depth. For each mooring, the depth in meters of the current meters is given in each column followed by the length of the time series in days. Only series longer than 120 days were used. The current-meter A3 record has gaps for unclear reasons and therefore was not used.

	Real depth (m); length of the time series (days)				
	S (0.75°S)	N (0.75°N)	A (equator)	Y_A (equator)	Y_B (equator)
1	840; 380	745; 375	825; 234	1187; 120	930; 257
2	1110; 42	1000; 377	1060; 339	1420; 120	1190; 258
3	1360; 272	1120; 294	1275; 148	1645; 120	1415; 258
4	1525; 248	1385; 257	1460; 378	1830; 120	1635; 12

The PIRATA wind dataset has also a daily temporal resolution and a record length of 377 days. There are, however, big gaps in the record (Fig. 6, top), and we therefore opted to perform a wavelet analysis (described in section 3) instead of the multitaper method analysis.

3. Wavelet analysis

To detect and extract quasiperiodic signals, we use a wavelet ridge analysis (Delprat et al. 1992; Mallat 1999) together with a reconstruction scheme. Details can be found in the appendix; here we give a general overview, emphasizing practical considerations. The problem is to isolate and reconstruct signals of the form

$$x_1(t) = A(t)\cos[\phi(t)] \tag{1}$$

for the case in which $\omega(t) = d\phi/dt$, known as the "instantaneous frequency," varies with time. Such signals,

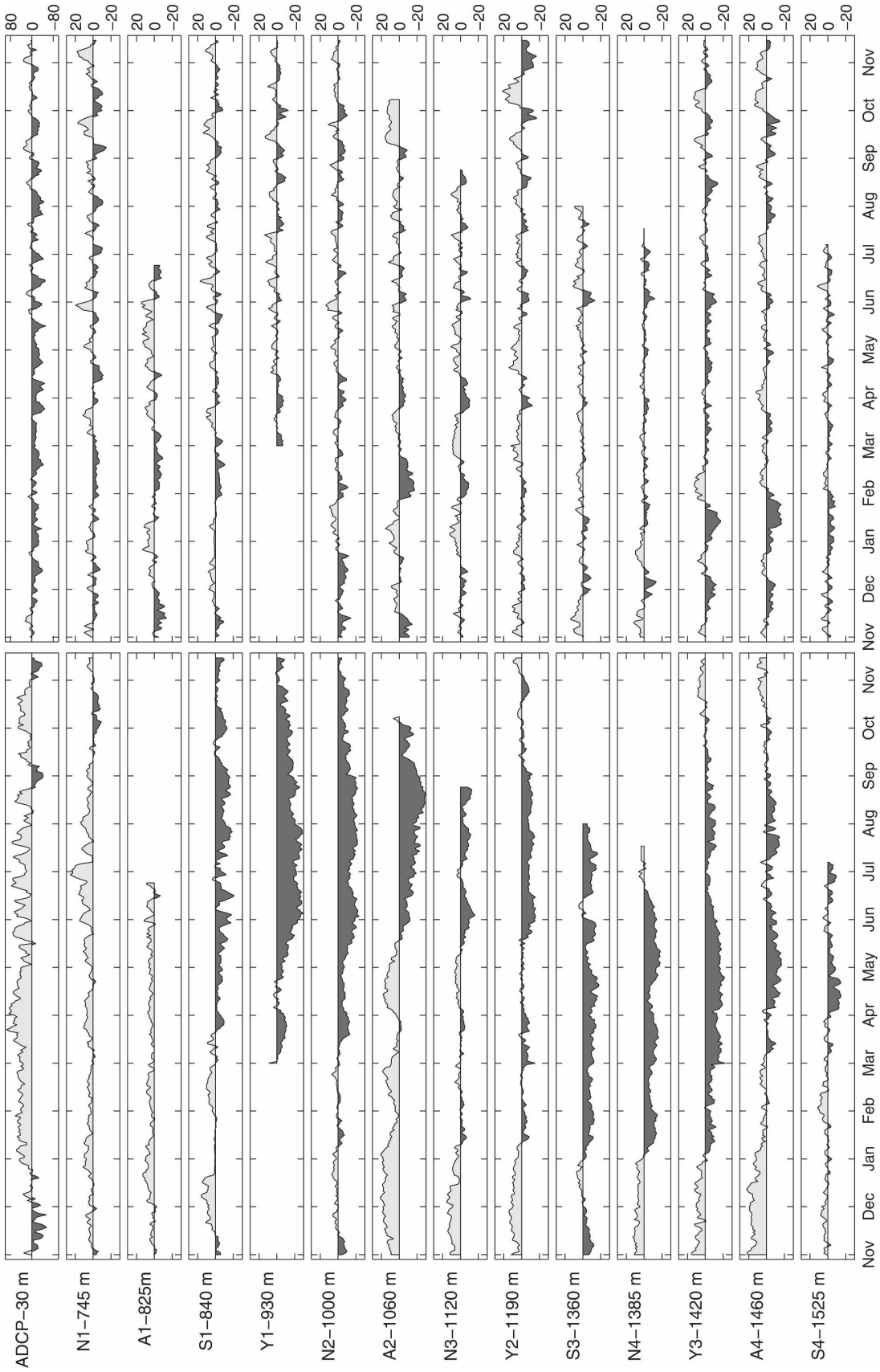

FIG. 3. (left) Zonal and (right) meridional velocity components (cm s^{-1}) obtained from the instrument array at 10°W. The letters to the left identify the mooring. Negative velocities (blackened areas) are westward and southward directions respectively. Time line starts on 12 Nov 1999 and ends on 24 Nov 2000.

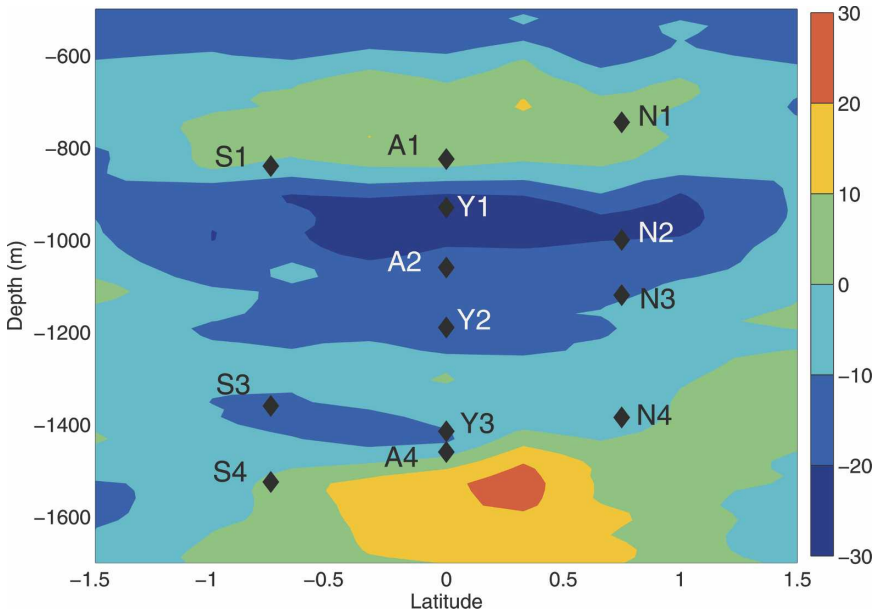

FIG. 4. Section of zonal velocity (cm s^{-1}) at 10°W. The section was made between 30 Jul and 1 Aug 2000 during an EQUALANT cruise. The vertical resolution is 16 m, and the spacing between LADCP stations is ⅓° between 1°S and 1°N and ½° elsewhere. The diamonds and labels correspond to the current-meter positions and names. Three clear jet structures are observed: 1) an eastward jet centered at 750 m with a meridional extension of 1° at each side of the equator, 2) a westward jet with maximum velocities at around 1000 m and a total meridional extension of 3°, and 3) an eastward jet with maximum velocities at 1550 m and a total extension of 2°. Between 1200 and 1400 m there is no clear signature of a deep jet structure.

which will be shown to be common in this dataset, are not well represented using Fourier analysis.

The wavelet transform of a time series (defined in the appendix) is a complex-valued function $W(t, s)$ of two variables, the time t and "scale" s. If a signal of the form (1) is present in a time series, its presence will be indicated by a curve $\tilde{s}(t)$, called a wavelet "ridge," on the time-scale plane. Ridges trace out the variations of the instantaneous frequency with time under assumptions of slow variations of $A(t)$ and $\omega(t)$, which are given explicitly in Delprat et al. (1992) or Mallat (1999). Such signals as (1) may be identified even if other variability is present at the same time, for example, sufficiently small-amplitude noise or other quasiperiodic signals at other sufficiently distant, frequencies. For our choices of normalization, discussed in the appendix, the ridge location reflects the instantaneous frequency of the signal (1) through $\tilde{s}(t) \approx 1/\omega(t)$, while the amplitude of the wavelet transform gives the signal amplitude $|W[t, \tilde{s}(t)]| \approx A(t)$. These approximations hold under the slowly varying assumptions and become exact for a constant sinusoidal signal.

After locating such signals, we wish to reconstruct them. The simplest way is to use the wavelet ridge location and amplitude to determine $A(t)$ and $\omega(t)$. However, this approach leads to sudden starts and stops of the reconstructed signal components, giving the appearance of a discontinuous behavior. Instead we use a different approach, described in the appendix, giving reconstructions that begin and end continuously and are smoother overall than those of the direct method.

It is also important to mention the "edge effects." At either end of the time series, the wavelet will extend past the end of the data, leading to edge effect regions—whose widths are proportional to the scale s—where the wavelet transform is contaminated. Edge effects are not problematic for this analysis because (i) we are using time-localized wavelets and (ii) there is not much low-frequency variability present near either endpoint of the time series. We tested the importance of the edge effects by using two different boundary conditions in the wavelet transform, in the first case setting the missing data to zeros and in the second "reflecting" the data about either endpoint. The difference between these two cases was generally minor, even within the edge-effect regions. We have chosen to present the results of the reflecting boundary condition method.

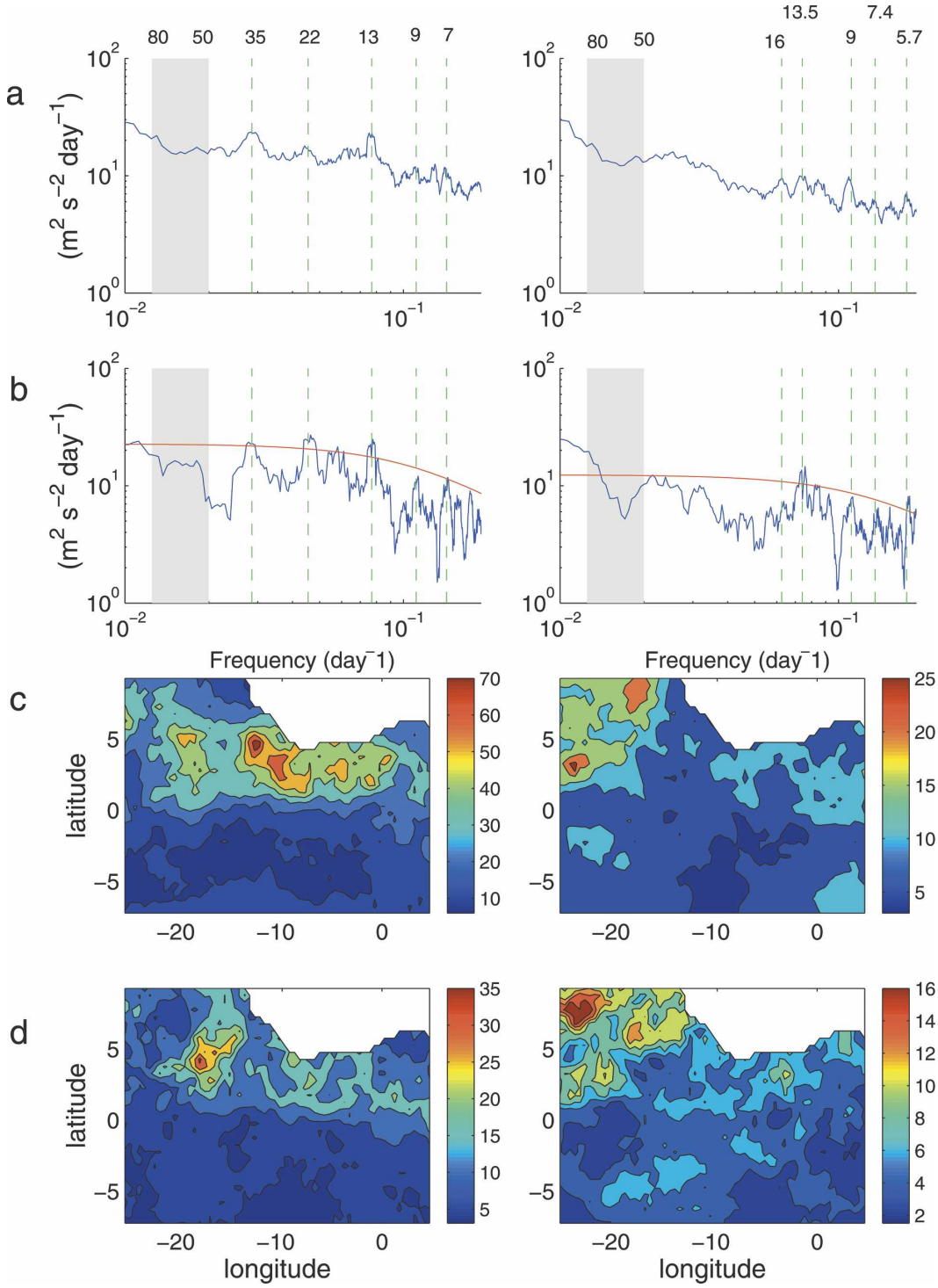

FIG. 5. (a) Mean velocity wind spectra of the (left) zonal and (right) meridional components from QuikSCAT. The mean is computed with the 2108 spectra corresponding to the grid points between 7.25°S and 9.25°N and between 25.75° and 0.25°W. The vertical lines from left to right indicate the periods of 35, 22, 13, 9, and 7 days (zonal component) and 16, 13.5, 9, 7.4, and 5.7 days (meridional component). Shadowed region indicates the 50–80-day band. (b) Same as (a) but for a point located at 0.25°N, 10.25°W. The red curve indicates the 95% confidence interval. (c), (d) Amplitude of the spectrum (left) for 13 and 7 days for the zonal component and (right) for 13.5 and 7.4 days for the meridional component.

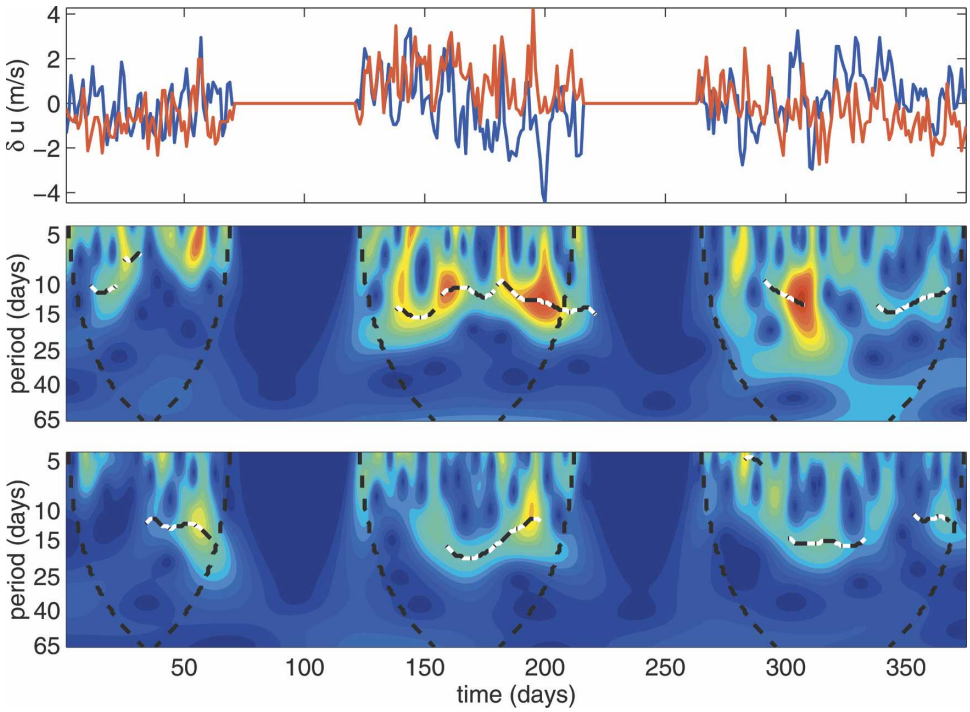

FIG. 6. (top) Normalized PIRATA buoy anomalies time series of the wind horizontal velocity components at 10°W (blue: zonal component; red: meridional component). Time line starts on 12 Nov 1999, coinciding with the time line of current-meter data. Data gaps are between 70 and 120 days (20 Jan–10 Mar), and between 214 and 264 days (12 Jun–1 Aug). Wavelet transform amplitude of the two series plotted above [(middle) zonal component and (bottom) meridional component]. The black and white lines are the ridges of maximum amplitude from which the main components are extracted to reconstruct the signal, as shown in Fig. 7. The dotted black lines indicate the cutoff region to avoid edge effects.

After locating all ridges of each time series, we choose two criteria to eliminate ridges that are likely to result from "noise" or are otherwise spurious. The first criterion retains oscillations with ridge amplitudes larger than a measure of high-frequency "noise-like" variability: for a ridge of temporal duration D_r and mean amplitude along the ridge $A_r = D_r^{-1}\int_{t_1}^{t_2} |W[t, \tilde{s}(t)]|dt$, where t_1 and t_2 are the start and end points of the ridge, A_r must be larger than σ_H, where σ_H is the standard deviation of the time series accounted for by Fourier components having periods of less than 7 days. The second criterion rejects short-duration events, since we are interested only in quasiperiodic features: only ridges with duration D_r greater than the period $1/\omega$ at the ridge point are selected.

This method was applied to each velocity component of the current-meter data and PIRATA wind data. The wavelet transform and the significant ridges on wind data at 10°W after extraction of the total mean (Fig. 6) show that the method successfully detects signals, even though large gaps are present in the time series shown in Fig. 6. The edge effects can be minimized by eliminating the wavelet region with less than half the length of the wavelet at each central frequency in each band (see dotted dark lines in Fig. 6).

To reconstruct the quasiperiodic signal in the 5–100-day band, we sum the reconstructions corresponding to the selected ridges in each time series. The results are displayed in Fig. 7; large amplitude variability in the meridional component is captured almost entirely, while the energetic large period events in the zonal component are not. Both components show a marked "seasonality" in the variability; in general, the first half of the series is dominated by longer periods than the second one.

The method is successful in isolating most of the organized quasiperiodic variability; the residuals (Fig. 8) consist of high-frequency noise and of some isolated fluctuations that were excluded either for belonging to short ridges ($D_r > 1/\omega$, e.g., the meridional component of A1 and A2) or for having periods outside the 5–100-day band (e.g., very low frequency variability in the zonal component).

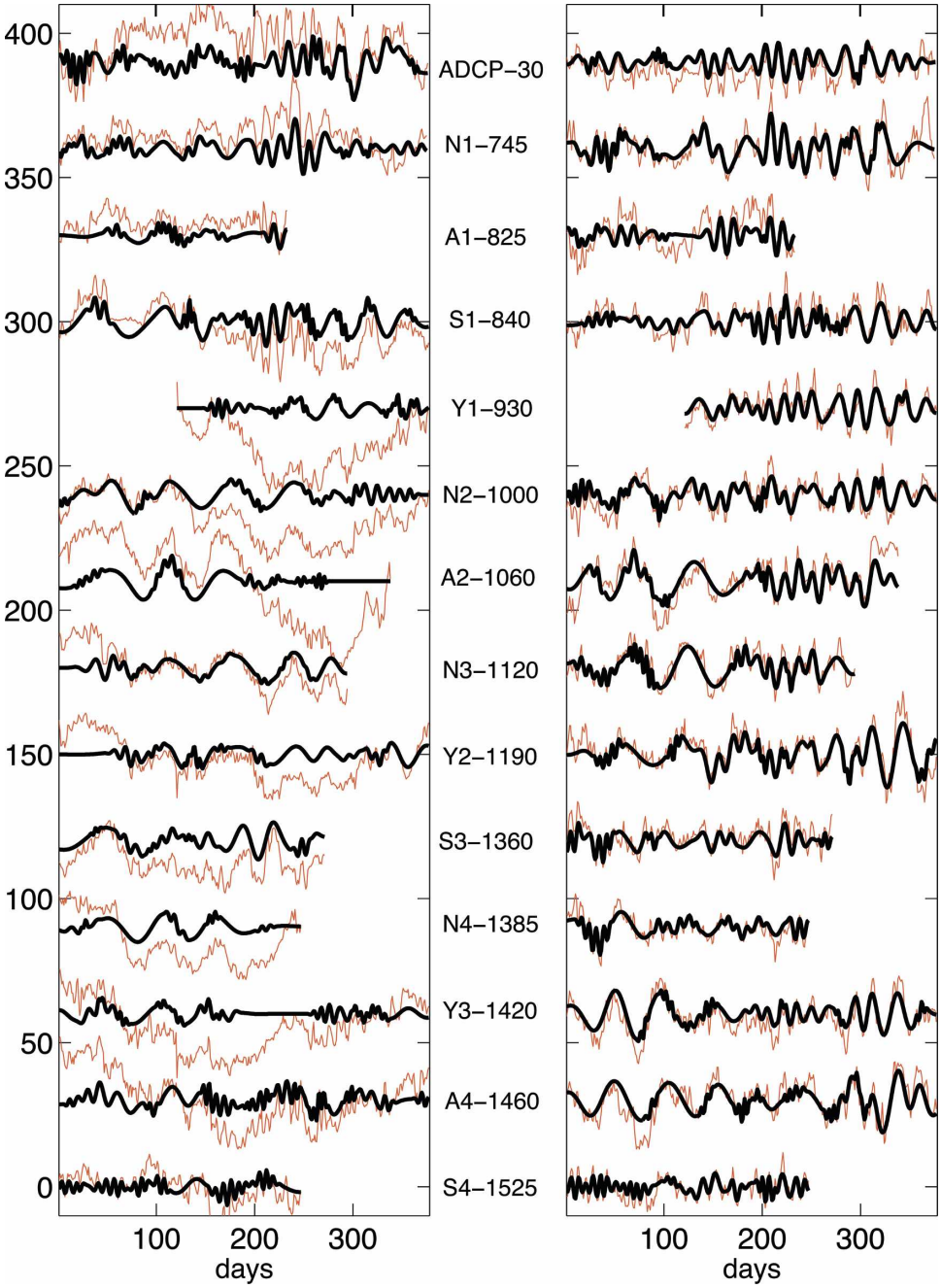

FIG. 7. (left) Zonal and (right) meridional velocity components (cm s^{-1}) obtained from the instrument array at 10°W (red). In black (thick) is the reconstructed signal of the 5–100-day period band from the wavelet analysis. Series are offset by a factor of 30 and the values of ADCP-30 series are divided by 4. The name and depth of each instrument is specified between the two plots. Time line starts 12 Nov 1999 and ends 24 Nov 2000. It is observed that single isolated oscillations are not picked up, either because they do not fulfill our "ridge criteria" or because the period of the events is out of the period band that is being extracted (5–100 days).

4. Observed periods

The histograms in Fig. 9 show the most important periods found in the water column; they represent the number of days in which events of each period occurred, summed over all current-meter series. This information comes directly from the selected ridges detected as described in section 3. The zonal component presents larger period variability than the meridional

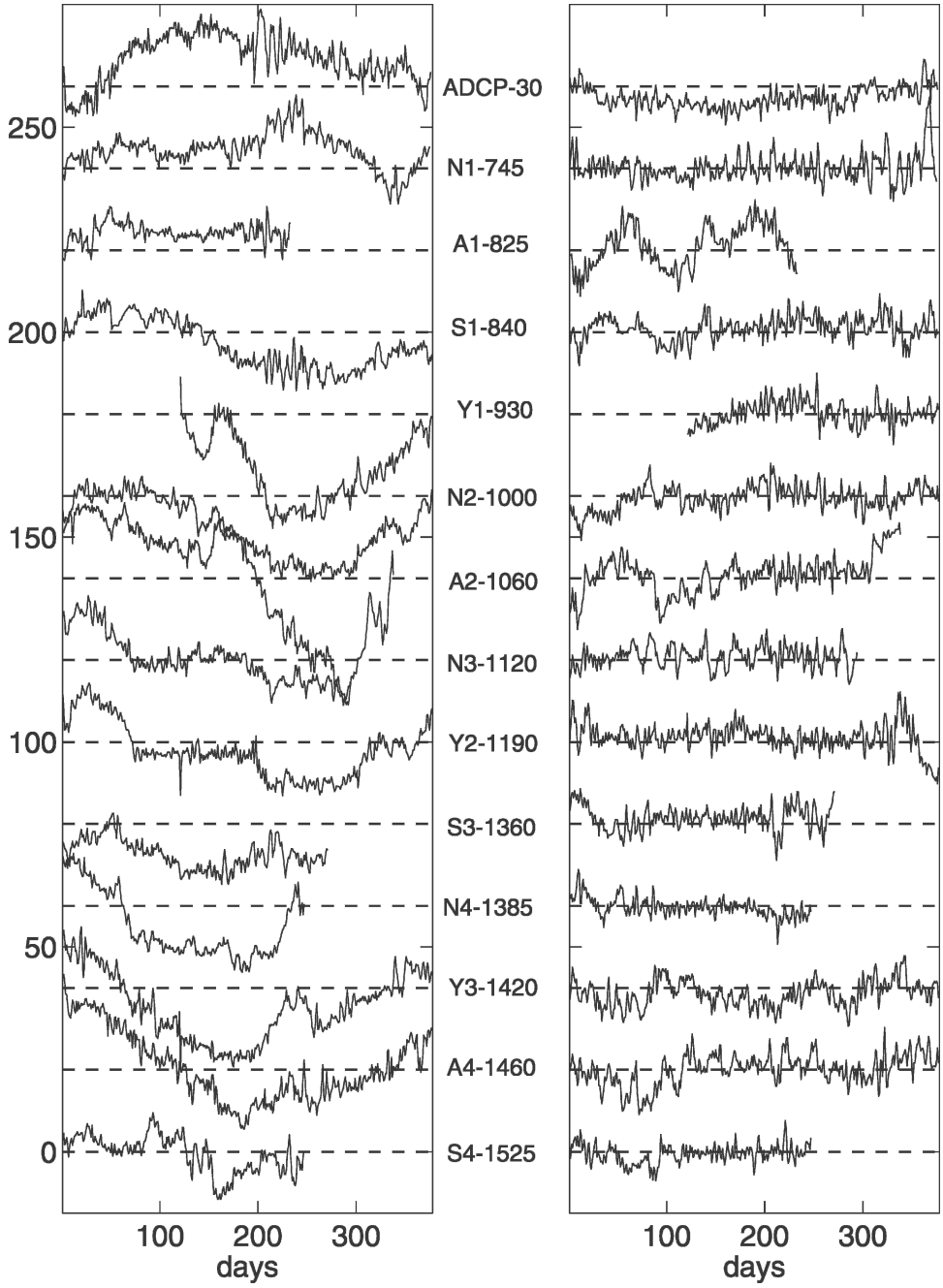

FIG. 8. Residues of (left) zonal and (right) meridional velocity component time series (cm s^{-1}) after subtraction of significant quasiperiodic oscillations with periods between 5 and 100 days. The series are offset by a factor of 20. The values of series ADCP-30 are divided by 4. The name and depth of each instrument is specified between the two plots. Time line starts 12 Nov 1999 and ends 24 Nov 2000. Some isolated oscillations in the 5–100-day period band have not been picked up because they do not fulfill our "ridge criteria" (e.g., see meridional component of A1–825). In other cases, the periods of the events observed are out of the 5–100-day range (e.g., most zonal component series).

component; especially noticeable are oscillations around 70 days. The meridional component shows two distinctive peaks, one at 14 days and the other at ~60 days. These histograms and previous information about the period of events found in the region (e.g., Garzoli 1987) suggest distinguishing the following period bands: 5–10 for the 7-day period oscillations, 10–20 for the 14-day period oscillations, 20–40 for the tropical insta-

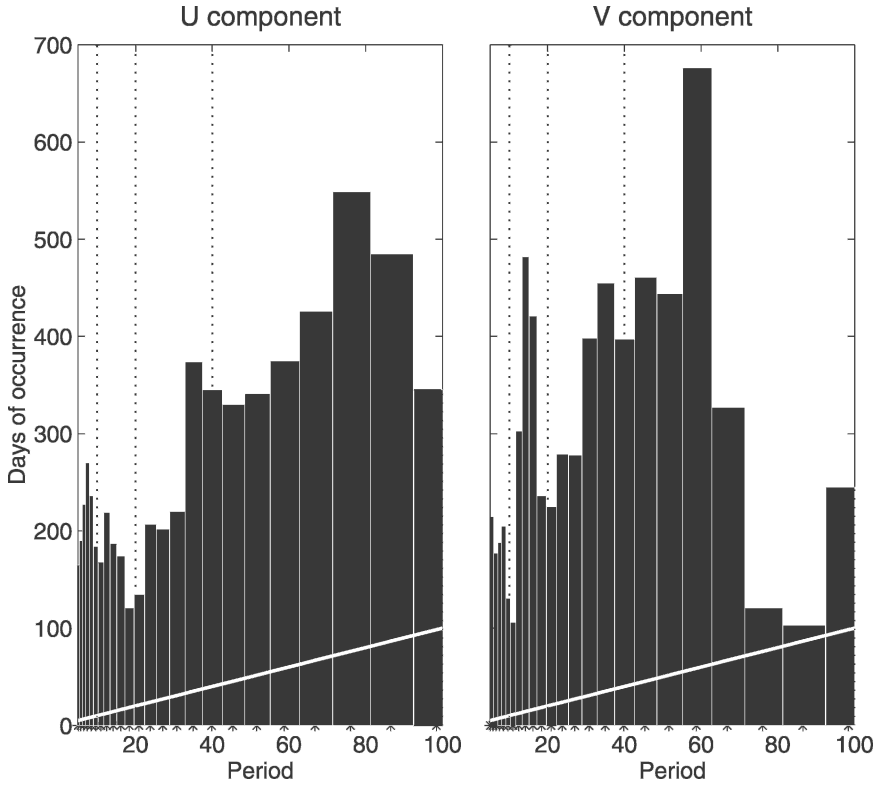

FIG. 9. Ridge histograms for the (left) zonal and (right) meridional velocity components of all current-meter data. The bins were constructed by choosing the inverse of the central frequency of the wavelets used to calculate the wavelet transform. Central frequencies of the wavelets follow a logarithmic progression in such way that $\Delta[\log(f)] = \text{const}$; therefore, bins from long periods are larger than those of short periods. The vertical dotted lines indicate the limits of the period bands considered (5–10, 10–20, 20–40, and 40–100 days). The white line indicates the portion of the bars equivalent to one cycle.

bility waves, and 40–100 for the 60- and 70-day period oscillations.

Figure 10 shows the signal corresponding to each period band for each velocity component. There is a marked seasonality, especially in the meridional component. Most time series can be divided in three parts: one with short periods in the middle and two with longer periods before and after. It is also observed that some oscillations are present in the entire water column, while others appear exclusively at certain depths and/or have distinctive behavior depending upon latitude. Examples of these are oscillations of ~14-day periods in the zonal component, which are only seen at the surface and at around 800 m (between 200 and 270 days of the time series), and oscillations of ~60-day periods in the meridional component, which are only present around 1100 and 1400 m.

The 5-yr satellite wind data were analyzed for the 5–100-day period band. The spectra present regional differences that explain why the mean of all spectra (Fig. 5a) differs from the spectrum at 0.25°N, 10.25°W (Fig. 5b). For the zonal wind data component, the most important periods are 7, 9, 13, 22, and 35 days and, for the meridional component, they are 5.7, 7.4, 9, 13.5, and 16 days. Interestingly, the amplitude of the spectra for some specific periods presents different spatial distributions for each velocity component. For example, the amplitude of the spectrum at 13 days in the zonal component is maximum in a region located between 0° and 6°N, 20°W and 0° (Fig. 5c, left), while the spectrum of the 13.5 days in the meridional component shows most of its energy in a region between 2° and 9°N, 25° and 15°W (Fig. 5c, right).

We now systematically describe the variability of the current-meter data in order of increasing period.

- *5–10 days*: Variability in this band presents a disorganized appearance, which in some cases can be defined as noise. Nevertheless, some features are worth mentioning. Near the surface, conspicuous events are only present in the zonal component (Fig. 10). At depth, oscillations within this period band are com-

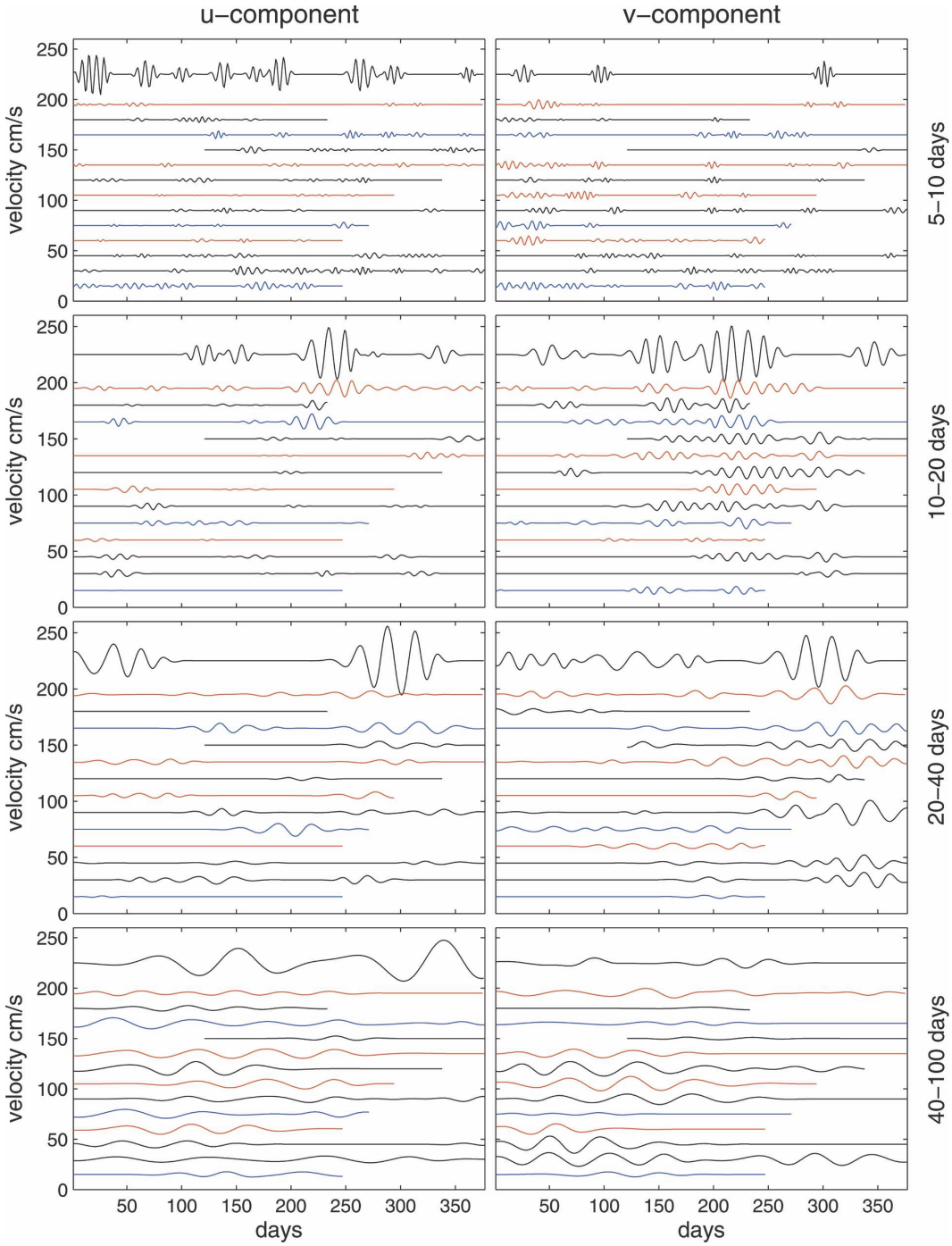

FIG. 10. Signal extracted in the different period bands (5–10, 10–20, 20–40 and 40–100 days, from top to bottom) for the (left) zonal and (right) meridional velocity components. The time series are in increasing order of depth (ADCP-30, N1–745, A1–825, S1–840, Y1–930, N2–1000, A2–1060, N3–1120, Y2–1190, S3–1360, N4–1385, Y3–1420, A4–1460, and S4–1525) and offset by 15 units, except for the surface where the offset is of 36 units; northern location series (red), southern location series (blue), and equatorial locations series (black). Time line starts 12 Nov 1999 and ends 24 Nov 2000.

mon along the year in the deepest VACM (S4) at 1525 m (hereinafter referred to as S4–1525) for both velocity components. In the meridional component, these oscillations also appear in the deeper southern and northern instruments (S3–1360, N4–1385, and S4–1525). During approximately the first 50 days of the records, they show opposite phases for northern and southern mooring locations, creating a converging/diverging flow at the equator. This is interesting because of the implied up and down vertical velocities in a region where deep waters should theoretically upwell. Unfortunately, there is not enough data to have a complete picture of the structure of the velocity field corresponding to this period. The lack of continuity with depth and the different times of occurrence of the signal suggest that the events near the surface and at depth are not related. Moreover, the relation between components is not explainable in most cases in terms of a single phenomenon because they occur at different times of the year.

- *10–20 days*: The principal oscillation in the 10–20-day band has a period of approximately 14 days. These oscillations are very energetic near the surface and are mainly observed during the end of the spring to midsummer (Fig. 10, 200–250 days). Near the surface, the signal is present in both velocity components at the equator, probably directly forced by the wind stress, which presents simultaneous fluctuations in the same period band (Fig. 6).

  In the meridional component, 14-day oscillations are observed in almost all VACM records with roughly the same seasonality (Fig. 10). However, in the zonal component, they are only visible in the upper VACM records (N1, A1, and S1). At those depths (~800 m), the structure of the signal is symmetric in the meridional component and antisymmetric in the zonal component (Fig. 10, N1–745 and S1–845), reminiscent of Rossby–gravity waves.

  Assuming that the observed variability corresponds to a Rossby–gravity wave, a number of parameters can be estimated: The linear theory of equatorial waves (e.g., Gill 1982) links the amplitude of the meridional velocity of the signal v_0 to the amplitude of the meridional shear of the zonal velocity component $\partial_y u$ through the relation $\partial_y u = v_0\omega/c$, where ω is the frequency of the wave and c is the phase speed of pure gravity waves of the vertical mode considered. According to the velocity records near the 800-m depth level, characteristic values of v_0, $\partial_y u$, and ω are $v_0 \approx 6$ cm s^{-1}, $\partial_y u \approx 6 \times 10^{-7}$ s^{-1}, and $\omega = 5.2 \times 10^{-6}$ s^{-1}; thus we obtain $c \approx 51$ cm s^{-1}, which corresponds to a vertical mode 4 or 5 for the Atlantic. This value of c is almost constant throughout the records where this calculation can be performed. For this value of c, the linear dispersion relation of a Rossby–gravity wave with a frequency $\omega = 5.2 \times 10^{-6}$s^{-1} shows eastward phase propagation. The Froude number Fr $= v_0/c$, which compares the magnitude of the advection terms with the propagation velocity of pure gravity waves, is approximately 0.1, therefore suggesting a weakly nonlinear behavior.

  The satellite wind data, as well as the PIRATA wind data, show high energy in this band in both horizontal velocity components (Fig. 5a and Fig. 6). At 10°W, satellite wind data shows that these fluctuations are stronger during spring and summer for both components and that the zonal component has, in general, larger amplitudes. In the zonal component, this signal has been associated with a near-surface westerly jet close to the African continent, whose latitudinal position varies with the meridional migration of the ITCZ (Grodsky et al. 2003). In the meridional component, satellite data show that this period is present in the western part of the basin, north of 2°N, but not as much in the Gulf of Guinea (Fig. 5c).
- *20–40 days*: Fluctuations with this period are observed primarily in August and September (Fig. 10). Near the surface, the periods of events are approximately 24 days. The zonal component has amplitudes up to 30 cm s^{-1}, while the meridional component has maximum amplitudes of 22 cm s^{-1}. At depth, the most conspicuous events in the zonal component are observed simultaneously to those near the surface in records S1 and Y1. Their period is approximately 34 days and therefore they cannot be directly related to near-surface events. In the meridional component, 20–40-day period fluctuations are seen in almost all VACMs a month later than the near-surface events. Periods are about 25 days in S1, Y1, N2, Y3, and A4, and 33 days in N1 and Y2 (Fig. 10). Fluctuations in the 20–40-day period band occurring in August–September within the mixed layer have been associated with tropical instability waves (e.g., Weisberg and Weingartner 1988).
- *40–100 days*: Near the surface, signals within this period band are conspicuous only in the zonal component. At depth, oscillations with these periods are mostly present in the first half of the series (from November 1999 to April 2000) for both velocity components (Fig. 10).

  The period of fluctuations observed in the zonal component at depth is mostly in the 60–80-day band. They are particularly important at intermediate depths (S1–840, N2–1000, A2–1060, and N3–1120) where they have amplitudes of 5–7 cm s^{-1}. The pres-

ence of these oscillations at 30 m in the first half of the series could suggest that the forcing of these waves comes from near the surface. Such variability is, however, not present in the satellite wind data analyzed here (Fig. 5a, shadowed area), and the PIRATA wind records cannot be used for this period band because of gaps in the time series.

At depth in the meridional component, oscillations within this period band are found exclusively in the northern and equatorial moorings, around 1100 and 1400 m, with amplitudes from 4 to 8 cm s^{-1} (Fig. 10) and a period of ~60 days. There is a clear opposition of phase between records at ~1100 m and those at ~1400 m. The phase relation between levels could be interpreted either as a vertical propagation or as a standing mode with a vertical scale of 600–800 m. The lack of signal in the southern mooring records implies that the geometry of the wave has no symmetry with respect to the equator or that the southern records coincide with nodes in the vertical. A possible forcing mechanism cannot be local and from the surface at the same time; there is no conspicuous signal in shallower records or in the wind field. However, variability with similar periodicities has been observed in northern Tropics (15°–25°N) wind data (Foltz and McPhaden 2004) and in subsurface eddies from the western boundary current in the tropical south Atlantic (Dengler et al. 2004). The potential link between all those observations, if it exists, is far from being understood.

5. Long-duration events: Evidence of an EDJ

Because the annual cycle is so important in the equatorial Atlantic, at the surface as well as at intermediate and great depths (Mercier and Speer 1998; Schmid et al. 2003; Brandt and Eden 2005; Böning and Kröger 2005; Thierry et al. 2006), it is reasonable to hypothesize that the observed low frequency (Fig. 8, zonal component) is the result of an annual signal plus the signature of other events of shorter vertical scale, like equatorial deep jets. The problem is to identify which variability corresponds to the EDJ and which to the annual signal. An annual signal suggesting a vertical mode 3 or 4 has been observed in current-meter data at depth at 15°W (Thierry 2000). Moreover, energetic large vertical scale phenomena are often seen in LADCP profiles (e.g., Fig. 1 of Ponte et al. 1990; Fig. 3 of Schott et al. 2003) and may be associated to this annual signal. On the other hand, the EDJ are known to have small vertical scales (400–600 m) and strong amplitudes (~10 cm s^{-1}). This relation corresponds to strong nonlinear features characterized by large Froude numbers, as estimated from published LADCP sections (e.g., Gouriou et al. 1999; Bourlès et al. 2003). The Froude number, $\mathrm{Fr} = U/c = Um/N$, is calculated with the mean Brunt–Väisälä frequency $N = 0.0023\ \mathrm{s}^{-1}$ (characteristic for those depths using data from the EQUALANT 2000 hydrographic data) and with the velocities and vertical wavelengths derived from the LADCP sections.

The vertical spacing between the current meters used in this study is small (90 m or less, with one exception between Y2–1190 and S3–1360 where the vertical spacing is 170 m), and therefore provides enough vertical resolution to study the EDJ and to answer the question as to whether the observed variability comes from the EDJ or larger vertical scale events. It is also important to consider the meridional spacing between current meters since current meters in the northern and southern positions could be located outside the jet region. A change in the direction of the flow in that case would represent a meridional scale rather than a vertical scale. Examination of LADCP sections in the depth range of 745–1525 m (Gouriou et al. 1999; Send et al. 2002; Bourlès et al. 2003) shows, however, that EDJs extend at least to 0.75°S and N of the equator (with smaller amplitude on either side of the equator) and are therefore adequately sampled by the moored array. The annual signal latitudinal extent is also larger than the mooring array since it is associated with the lowest odd meridional mode Rossby beam (e.g., Brandt and Eden 2005).

Most zonal-component time series present low-frequency variability (Figs. 3 and 7) that clearly appears in the residues after extraction of the significant high-frequency signals (Fig. 8). These long-period fluctuations obey neither a standing mode pattern (where changes in phase are of 180°) nor a vertical propagation pattern (changes in phase are not monotonic). Moreover, the phase of the fluctuations seems to depend upon depth and not upon latitude.

At 745 m (N1–745), the residual zonal component has a maximum eastward velocity of 15 cm s^{-1} around mid-July 2000. Approximately at the same time and 255 m deeper (N2–1000), the flow is westward with a maximum velocity of 20 cm s^{-1}. The vertical scales as well as the magnitude of the velocities correspond well with the signature of EDJs. Moreover, the depth, magnitude, and direction of these flows compare well with the LADCP measurements made in July–August 2000 (Fig. 6). The Froude number is calculated as above with a maximum amplitude for the jet velocity of 0.15 m s^{-1} and a vertical wavelength $m = (2\pi/510)\ \mathrm{m}^{-1}$. It is approximately equal to 0.8, a value comparable to those estimated from the LADCP sections.

These two depths (745 and 1000 m) do not always have zonal flows in opposite directions. At the beginning of the measurements, from mid-November 1999 to

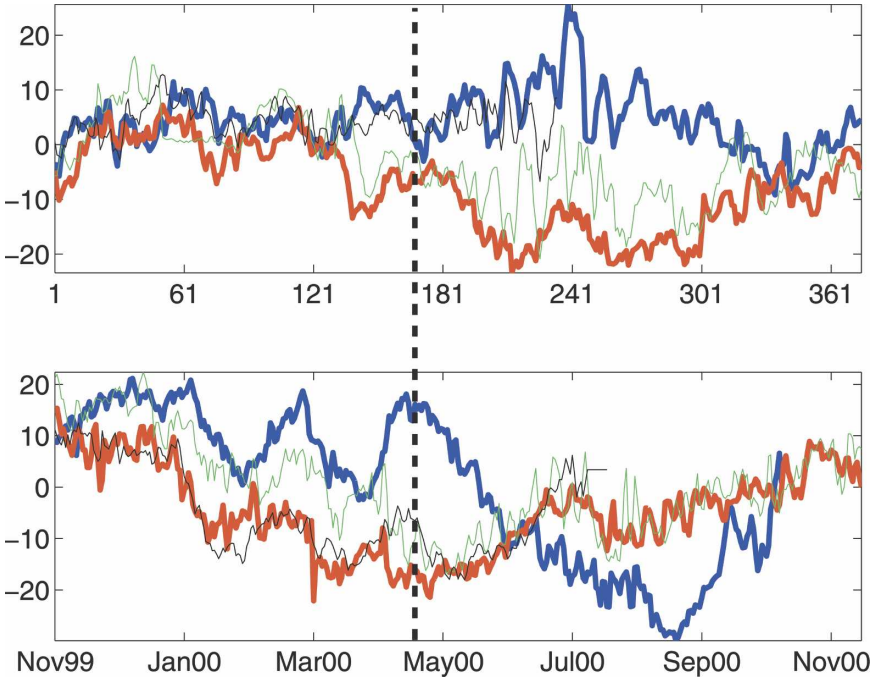

FIG. 11. Daily zonal velocity component (cm s^{-1}). (top) VACM N1–745 (blue), A1–825 (black), S1–840 (green), and N1–1000 (red); (bottom) VACM A2–1060 (blue), N4–1385 (black), Y3–1420 (red), and A3–1460 (green). Thick lines indicate records from the same latitude with the higher opposite velocities. The black dotted line shows the time of maximum shear between A2 and Y3, discussed in the last section of the manuscript. The *x* axis on top is in days (starting 12 Nov 1999 and ending Nov 2000) and the one in the bottom indicates the month and year.

mid-February 2000, the flow at both depths (as well as at A1–825, S1–840) is eastward with a velocity of 3 cm s^{-1} (Fig. 11, top). Then the two series show zonal velocities in opposite direction for approximately 220 days and then again in the same direction by mid-October until the end of the record. The data records from instruments at intermediate depths between N1 and N2 (A1–825, S1–840, and Y1–930) exhibit the same behavior: A1–825, although lacking some data, suggests a node around that depth (Fig. 11, top, cyan line); S1–840 shows a similar pattern to that of N2, but slightly shifted to more positive velocity values, probably because of its shallower depth (Fig. 11, top, green line); and Y1–930 shows stronger westward flow than N2 (Fig. 8), probably because of its location at the equator where the jet velocities are stronger (Fig. 4). All of these records (N1, A1, S1, Y1, and N2) present similar zonal velocity values at their beginning (from November 1999 to February 2000) and end (from October to November 2000). One possible explanation is that these two EDJs have an intermittent behavior and a lifetime of around 7–8 months, a time scale much shorter than those estimated in the western tropical Atlantic (at least 5 yr according to Johnson and Zhang 2003). The observations of Weisberg and Horigan (1981) in the eastern tropical Atlantic between 600 and 1800 m suggest similar vertical and temporal scales for the zonal component to those of our observations: 365 m and 4–8 months.

Between the records at the equator, A2–1060 and Y3–1420, there is also a vertical shear of the zonal component over 360-m depth, lasting 7–8 months (from November 1999 to June 2000, Figs. 8 and 11, bottom). This shear is modulated by ~70 day oscillations and may be as strong as 40 cm s^{-1} in 360 m of depth in April 2000 (Fig. 11, bottom). The implied vertical scale, 720 m, is larger than the 400–600-m scale of EDJs in the Atlantic. Nonetheless, the Froude number is high (Fr $\approx$ 0.8), like in EDJ structures.

6. Summary and discussion

New velocity data from surface and intermediate depths are presented. We analyze these data using a wavelet-based method to extract quasiperiodic variability in the 5–100-day band. The results were classified in four bands: 5–10, 10–20, 20–40, and 40–100 days, for both horizontal velocity components.

Near the surface, the 7-day period oscillations are most probably forced by the wind stress. The satellite

wind data show a peak of energy at around 7 days (Figs. 5a and 5b) and the wavelet transform for the 1-yr PIRATA wind data at 10°W shows energy at those periods during December 1999–January 2000 (Fig. 6). This period was also observed by Colin and Garzoli (1988) in wind time series taken at 1°N, 29°W and 0°, 4°W and was associated with a harmonic of a biweekly signal. The amplitude of the spectrum of the wind zonal component for this peak has a spatial distribution that resembles that of 13 days (Figs. 5c and 5d), with a maximum in the latitudinal band, 0°–6°N, which supports Colin and Garzoli's (1988) findings.

Biweekly fluctuations are present simultaneously near the surface and at depth. Although such fluctuations are present in the wind velocity field, there is no clear pathway to the deep ocean. The 14-day period oscillations are especially present in the Gulf of Guinea at the surface (Houghton and Colin 1987) and have been observed at depth on the continental slope off the Angola coast (Vangriesheim et al. 2005).

Oscillations with periods of approximately 24 days are observed near the surface during August and September. These periods and their timing in the year correspond well with the signature of tropical instability waves in the Atlantic (e.g., Grodsky et al. 2005). A month later, at depth, oscillations with the same period are observed in the meridional component. However, it is not clear whether the 24-day period oscillations near the surface can be directly related to the fluctuations at depth. Model studies did, however, find a variety of short period fluctuations forced by instabilities of zonal currents on the equator (e.g., McCreary and Yu 1992), and we can therefore surmise that part of the variability found at depth is forced by similar instabilities. This could also explain the marked seasonality observed in the time series with the different period fluctuations throughout the year resulting from changes in currents strengths.

The 40–100-day period oscillations are very energetic at intermediate depths and are responsible for important vertical shears in the velocity components. In the meridional component, periods are approximately 60 days and the resulting shears due to opposite phase of the signal between depths can be as large as 15 cm s^{-1} over 360 m. In the zonal component, examples are the 50-day period oscillations present at the start of the 510-m vertical scale 8-month event and the 70-day period oscillations observed in A2–1060 (Fig. 11). Whether these 50- and 70-day period oscillations are dynamically linked to the EDJ or not, they can drastically change the vertical shear between two depths. According to the current-meter data, a LADCP section made during April 2000 would have shown a totally different picture of the jets than the one from August 2000 shown in Fig. 4 (see Fig. 11, black dotted line); in April 2000, there would be no vertical shear in the zonal component between 745 and 1000 m, and strong opposite flows between 1060 and 1420 m.

Despite recent works by Thierry et al. (2006) and Brandt and Eden (2005), the structure of the annual signal in the water column and its variation with longitude remains poorly known. In all of these studies, the phase of the annual signal is observed to change monotonically with depth. The low frequency observed in the records presented here does not fit this behavior and, on the contrary, suggests that, if an annual signal is present, it is masked by the presence of EDJs.

Events of long duration show two particularly interesting vertical scales: one of 510 m and another one of 720 m, both defined by the moorings vertical spacing. The first vertical scale is likely related to the EDJ since comparisons between the current-meter velocity measurements and LADCP data taken around 1 August 2000 (Fig. 4) show that the amplitudes, directions, and positions associated with the 510-m vertical scale agree with each other: both datasets exhibit an eastward jet at 745 m and a westward one at 930–1000 m. In that case, the current-meter time series suggests that the EDJs at 10°W are intermittent with time scales of approximately 7 months. In the case of the 720-m vertical scale, the velocities from both datasets also coincide, but there is no obvious jet at 1420 m in the August 2000 LADCP data. Despite the fact that the suggested vertical scale of 720 m is larger than commonly accepted (i.e., 400–600 m), the strong nonlinearity of the event ($Fr \approx 0.8$ in April 2000) is indicative of a jetlike structure. It is more difficult to estimate a time scale for the 720-m vertical scale owing to large uncertainties associated with the vertical sampling between Y2–1190 and S3–1360: some vertical displacement of the jets may have not been sampled by the array. However, as for the 510-m vertical scale, the zonal velocity shear reversal between time series A2–1060 and Y3–1420 suggests a time scale of around 7–8 months (Fig. 11, bottom).

The information content in the current-meter time series therefore suggests that the EDJs at 10°W have shorter time scales than those estimated by Johnson and Zhang (2003) and Send et al. (2002) for the western tropical Atlantic and have similar time scales to those estimated by Weisberg and Horigan (1981) in the eastern Atlantic. The methods used in estimations of EDJ time scales vary considerably, even in the cases in which current-meter data were used. Weisberg and Horigan (1981) performed a statistical analysis of their measurements and obtained a temporal scale of 4–8 months and a vertical scale of 365 m. However, at first glance, it is difficult to identify any jetlike structure in their data.

Send et al. (2002) fit an a priori model consisting of jets with a fixed vertical scale of 550 m to their mooring data, checked for the vertical phase of the jet system afterward, and then found an interannual temporal scale for the EDJ. Nonetheless, vertical shear corresponding to shorter time scales can be observed in their Fig. 11. In this paper, the high vertical resolution of the mooring array allowed us to make direct observations of the duration of vertical shears between two given depths. When comparing the three approaches, it is clear that the results depend greatly on the chosen method of analysis: the measurements of Send et al. (2002) may have yielded the same range of time scales if the statistical method of Weisberg and Horigan (1981) had been applied and vice versa. This raises the question of how one truly defines the time variability of the jets. Should all jets in the water column be coherent in time? Should a jet be considered the same one if the vertical shear between two depths disappears for a while and then reappears in the same direction? As long as the mechanism for the formation of EDJs remains unknown, it is not easy to provide an answer.

Acknowledgments. This research was funded by Institut de Recherche pour le Développement (IRD) and the national Programme Atmosphère et Océans Multiéchelles (PATOM). We thank the crew from R/V *Antea* (mooring deployment), R/V *Le Suroit* (mooring recovery and deployment), and R/V *Atlante* (mooring recovery). We warmly thank Sabine Arnault, Gilles Reverdin, Eric Chassignet, and the three reviewers for their useful comments and Lien Hua for her fruitful and stimulating discussions.

APPENDIX

Signal Detection and Reconstruction

The wavelet transform of a time series $x(t)$ is a function of time t and "scale" s

$$W(t, s) = \int \overline{\psi}_{t,s}(t')x(t')\,dt' \tag{A1}$$

and is formed by projecting the time series onto a set of functions $\psi_{t',s}(t)$ called "wavelets"; here the overbar is the complex conjugate. The wavelets $\psi_{t',s}(t)$ are shifted and rescaled versions of a zero-mean, finite energy "mother wavelet" function $\psi(t)$,

$$\psi_{t',s}(t) \equiv \frac{c}{s}\psi\left(\frac{t - t'}{s}\right), \tag{A2}$$

where c is a constant chosen as

$$c = \frac{2}{\int \psi(t')e^{-2\pi i t'}\,dt'}. \tag{A3}$$

The combination of this choice of c together with the scale normalization s^{-1} in (A2) has the property that the wavelet transform of a unit amplitude sinusoid of frequency f_0 has unit amplitude at scale $s = 1/f_0$.

The wavelets used here are "analytic wavelets," meaning that their Fourier transforms vanish for negative frequencies. The wavelet transform is then complex valued, even for a real-valued time series $x(t)$, so we write

$$W(t, s) = |W(t, s)|e^{i\theta(t,s)}, \tag{A4}$$

where $|W(t, s)|$ is the transform amplitude at the point (t, s) and $\theta(t, s)$ is its phase. Ridges are diagnosed directly from the wavelet transform phase $\theta(t, s)$ by finding connected curves such that

$$\frac{d}{dt}\theta[t, \tilde{s}(t)] = \frac{1}{\tilde{s}(t)}, \tag{A5}$$

which states that the rate of change of the wavelet transform phase at scale $\tilde{s}(t)$ is equal to the frequency associated with that scale.

Specifically, we use the generalized Morse wavelets of Olhede and Walden (2002), with parameter choices, $\beta = 2$ and $\gamma = 4$ (defined therein), which control the behavior of the wavelet's Fourier transform at low and high frequencies, respectively. This choice of parameters reflects a subjective assessment of which parameter settings best captured the variability present in the data.

To reconstruct a time series from its continuous wavelet transform involves integrating over the entire (t, s) plane. It is natural to attempt to reconstruct the quasiperiodic components (1) by limiting the reconstruction integral to a wavelet ridge. This is motivated by the fact that the wavelet transform is a two-dimensional smoothing of a more fundamental quantity, the Wigner–Ville distribution, which represents any linear chirp as a delta function (Mallat 1999). Following this suggestion, we write the "ridge reconstruction equation"

$$\hat{x}(t) \equiv \int W[t', \tilde{s}(t)]\psi_{\tilde{s}(t)}(t' - t)\,dt', \tag{A6}$$

which exactly reconstructs a sinusoid, and performed well in our numerical trials with slowly varying quasiperiodic signals.

REFERENCES

Boebel, O., C. Schmid, and W. Zenk, 1999: Kinematic elements of Antarctic Intermediate Water in the western South Atlantic. *Deep-Sea Res. II,* **46,** 355–392.

Böning, C. W., and J. Kröger, 2005: Seasonal variability of deep currents in the equatorial Atlantic: A model study. *Deep-Sea Res. I,* **52,** 99–121.

Bourlès, B., and Coauthors, 2003: The deep currents in the Eastern Equatorial Atlantic Ocean. *Geophys. Res. Lett.,* **30,** 8002, doi:10.1029/2002GL015095.

Brandt, P., and C. Eden, 2005: Annual cycle and interannual variability of the mid-depth tropical Atlantic Ocean. *Deep-Sea Res. I,* **52,** 199–219.

Colin, C., and S. Garzoli, 1988: High frequency variability of in situ wind, temperature and current measurements in the equatorial Atlantic during the FOCAL/SEQUAL experiment. *Oceanol. Acta,* **11,** 139–148.

Delprat, N., B. Escudié, P. Guillemain, R. Kronland-Martinet, P. Tchamitchian, and B. Torrésami, 1992: Asymptotic wavelet and Gabor analysis: Extraction of instantaneous frequencies. *IEEE Trans. Inf. Theory,* **38,** 644–665.

Dengler, M., F. A. Schott, C. Eden, P. Brandt, J. Fischer, and R. J. Zantopp, 2004: Break-up of the Atlantic deep western boundary current into eddies at 8°S. *Nature,* **432,** 1018–1020.

Eriksen, C. C., 1985: Moored observations of deep low-frequency motions in the central Pacific Ocean: Vertical structure and interpretation as equatorial waves. *J. Phys. Oceanogr.,* **15,** 1085–1113.

Firing, E., 1987: Deep zonal currents in the central equatorial Pacific. *J. Mar. Res.,* **45,** 791–812.

Foltz, G. R., and M. J. McPhaden, 2004: The 30–70 day oscillations in the tropical Atlantic. *Geophys. Res. Lett.,* **31,** L15205, doi:10.1029/2004GL020023.

Garzoli, S. L., 1987: Forced oscillations on the equatorial Atlantic basin during the Seasonal Response of the Equatorial Atlantic Program (1983–1984). *J. Geophys. Res.,* **92,** 5089–5100.

Ghil, M., and Coauthors, 2002: Advanced spectral methods for climatic time series. *Rev. Geophys.,* **40,** 1003, doi:10.1029/2000RG000092.

Gill, A. E., 1982: *Atmosphere–Ocean Dynamics.* Academic Press, 661 pp.

Gouriou, Y., B. Bourlès, H. Mercier, R. Chuchla, 1999: Deep jets in the equatorial Atlantic Ocean. *J. Geophys. Res.,* **104** (C9), 21 217–21 226.

——, and Coauthors, 2001: Deep circulation in the equatorial Atlantic Ocean. *Geophys. Res. Lett.,* **28,** 819–822.

Grodsky, S. A., J. A. Carton, and S. Nigam, 2003: Near surface westerly wind jet in the Atlantic ITCZ. *Geophys. Res. Lett.,* **30,** 2009, doi:10.1029/2003GL017867.

——, ——, C. Provost, J. Servain, J. A. Lorenzzeti, and M. J. McPhaden, 2005: Tropical instability waves at 0°N, 23°W in the Atlantic: A case study using Pilot Research Moored Array in the Tropical Atlantic (PIRATA) mooring data. *J. Geophys. Res.,* **110,** C08010, doi:10.1029/2005JC002941.

Houghton, R. W., and C. Colin, 1987: Wind driven meridional eddy heat flux in the Gulf of Guinea. *J. Geophys. Res.,* **92,** 10 777–10 786.

Hua, B. L., D. W. Moore, and S. Le Gentil, 1997: Inertial nonlinear equilibration of equatorial flows. *J. Fluid Mech.,* **331,** 345–371.

Johnson, G. C., and D. Zhang, 2003: Structure of the Atlantic Ocean equatorial deep jets. *J. Phys. Oceanogr.,* **33,** 600–609.

Kartavtseff, A., 2002: Mouillages EQUALANT. Rapport Interne LODYC 2002-02, 204 pp.

Lumpkin, R., and S. L. Garzoli, 2005: Near-surface circulation in the tropical Atlantic Ocean. *Deep-Sea Res. I,* **52,** 495–518.

Luyten, J. R., and J. C. Swallow, 1976: Equatorial undercurrents. *Deep-Sea Res. Oceanogr. Abstr.,* **23,** 999–1001.

Mallat, S., 1999: *A Wavelet Tour of Signal Processing.* 2d ed. Academic Press, 637 pp.

McCreary, J. P., and Z. Yu, 1992: Equatorial dynamics in a 2½-layer model. *Progress in Oceanography,* Vol. 29, Pergamon, 61–132.

Mercier, H., and K. G. Speer, 1998: Transport of bottom water in the Romanche fracture zone and the Chain fracture zone. *J. Phys. Oceanogr.,* **28,** 779–790.

Molinari, R. L., S. L. Garzoli, and R. W. Schmitt, 1999: Equatorial currents at 1000 m in the Atlantic Ocean. *Geophys. Res. Lett.,* **26,** 361–363.

Muench, J. E., E. Kunze, and E. Firing, 1994: The potential vorticity structure of equatorial deep jets. *J. Phys. Oceanogr.,* **24,** 418–428.

Olhede, S. C., and A. T. Walden, 2002: Generalized Morse wavelets. *IEEE Trans. Sig. Process.,* **50,** 2661–2670.

Percival, D. B., and A. T. Walden, 1993: *Spectral Analysis for Physical Applications—Multitaper and Conventional Univariate Techniques.* Cambridge University Press, 580 pp.

Philander, S. G. H., 1990: *El Niño, La Niña, and the Southern Oscillation.* Academic Press, 289 pp.

Ponte, R. M., J. Luyten, and P. L. Richardson, 1990: Equatorial deep jets in the Atlantic Ocean. *Deep-Sea Res.,* **37,** 711–713.

Richardson, P. L., and D. Walsh, 1986: Mapping climatological seasonal variations of surface currents in the tropical Atlantic using ship drifts. *J. Geophys. Res.,* **91,** 10 537–10 550.

——, and W. J. Schmitz, 1993: Deep cross-equatorial flow in the Atlantic measured with SOFAR floats. *J. Geophys. Res.,* **98,** 8371–8387.

Schmid, C., Z. Garraffo, E. Johns, and S. L. Garzoli, 2003: Pathways and variability at intermediate depths in the tropical Atlantic. *Interhemispheric Water Exchange in the Atlantic Ocean*, G. Goni and P. Malanotte-Rizzoli, Eds., Elsevier Oceanography Series, Vol. 68, Elsevier, 233–268.

Schott, F. A., and Coauthors, 2003: The zonal currents and transports at 35°W in the tropical Atlantic. *Geophys. Res. Lett.,* **30,** 1349, doi:10.1029/2002GL016849.

Send, U., C. Eden, and F. Schott, 2002: Atlantic equatorial deep jets: Space–time structure and cross-equatorial fluxes. *J. Phys. Oceanogr.,* **32,** 891–902.

Thierry, V., 2000: Observation et modélisation de la variabilité saisonnière dans l'océan Atlantique équatorial profond. Ph.D. thesis, Université de Bretagne Occidentale, 203 pp.

——, A. M. Treguier, and H. Mercier, 2006: Seasonal fluctuations in the deep central equatorial Atlantic Ocean: A data–model comparison. *Ocean Dyn.,* in press.

Thomson, D. J., 1982: Spectrum estimation and harmonic analysis. *Proc. IEEE,* **70,** 1055–1096.

Vangriesheim, A., A. M. Treguier, and G. Andre, 2005: Biweekly current oscillations on the continental slope of the Gulf of Guinea. *Deep-Sea Res. I,* **52,** 2168–2183.

Weisberg, R. H., and A. M. Horigan, 1981: Low-frequency variability in the equatorial Atlantic. *J. Phys. Oceanogr.,* **11,** 913–920.

——, and T. J. Weingartner, 1988: Instability waves in the equatorial Atlantic Ocean. *J. Phys. Oceanogr.,* **18,** 1641–1657.

——, A. M. Horigan, and C. Colin, 1979: Equatorially trapped Rossby-gravity wave propagation in the Gulf of Guinea. *J. Mar. Res.,* **37,** 67–86.